4.4   Thermal and Hydraulic Design

The thermal and hydraulic design of the reactor core provides adequate heat transfer compatible with the heat generation distribution in the core. This provides adequate heat removal by the reactor coolant system, the normal residual heat removal system, or the passive core cooling system.

4.4.1   Design Basis

The following performance and safety criteria requirements are established for the thermal and hydraulic design of the fuel. Condition I, II, III, and IV transients and events through out this section are as defined in ANSI N18.2a-75 (Reference 1).

- Fuel damage (defined as penetration of the fission product barrier; that is, the fuel rod clad) is not expected during normal operation and operational transients (Condition I) or any transient conditions arising from faults of moderate frequency (Condition II). It is not possible, however, to preclude a very small number of rod failures. These are within the capability of the plant cleanup system and are consistent with the plant design bases.

- The reactor can be brought to a safe state following a Condition III event with only a small fraction of fuel rods damaged (as defined in the above definition), although sufficient fuel damage might occur to preclude resumption of operation without considerable outage time.

- The reactor can be brought to a safe state and the core can be kept subcritical with acceptable heat transfer geometry following transients arising from Condition IV events.

To satisfy these requirements, the following design bases have been established for the thermal and hydraulic design of the reactor core.

4.4.1.1   Departure from Nucleate Boiling Design Basis

4.4.1.1.1 Design Basis

There is at least a 95-percent probability at a 95-percent confidence level that departure from nucleate boiling (DNB) does not occur on the limiting fuel rods during normal operation and operational transients and any transient conditions arising from faults of moderate frequency (Condition I and II events).

4.4.1.1.2 Discussion

The design method employed to meet the DNB design basis for the AP1000 fuel assemblies is the Revised Thermal Design Procedure, WCAP-11397-P-A (Reference 2). With the Revised Thermal Design Procedure methodology, uncertainties in plant operating parameters, nuclear and thermal parameters, fuel fabrication parameters, computer codes, and DNB correlation predictions are considered statistically to obtain DNB uncertainty factors. Based on the DNB uncertainty factors, Revised Thermal Design Procedure design limits departure from nucleate boiling ratio (DNBR) values are determined such that there is at least a 95-percent probability at a 95-percent confidence level that DNB will not occur on the most limiting fuel rod during normal operation and

operational transients and during transient conditions arising from faults of moderate frequency (Condition I and II events).

Assumed uncertainties in the plant operating parameters (pressurizer pressure, primary coolant temperature, reactor power, and reactor coolant system flow) are evaluated. Only the random portion of the plant operating parameter uncertainties is included in the statistical combination. Instrumentation bias is treated as a direct DNBR penalty. Since the parameter uncertainties are considered in determining the Revised Thermal Design Procedure design limit DNBR values, the plant safety analyses are performed using input parameters at their nominal values.

For those transients that use the VIPRE-01 computer program (subsection 4.4.4.5.2) and the WRB-2M correlation (subsection 4.4.2.2.1), the Revised Thermal Design Procedure design limits are 1.25 for the typical cell and 1.25 for the thimble cell for Core and Axial Offset Limits and 1.22 for the typical cell and 1.21 for the thimble cell for all other RTDP transients. These values may be revised (slightly) when plant specific uncertainties are available.

To maintain DNBR margin to offset DNB penalties such as those due to fuel rod bow (as described in subsection 4.4.2.2.5), the safety analyses are performed to DNBR limits higher than the design limit DNBR values. The difference between the design limit DNBRs and the safety analysis limit DNBRs results in DNBR margin. A portion of this margin is used to offset rod bow and unanticipated DNBR penalties.

The Standard Thermal Design Procedure is used for those analyses where the Revised Thermal Design Procedure is not applicable. In the Standard Thermal Design Procedure method the parameters used in analysis are treated in a conservative way from a DNBR standpoint. The parameter uncertainties are applied directly to the plant safety analyses input values to give the lowest minimum DNBR. The DNBR limit for Standard Thermal Design Procedure is the appropriate DNB correlation limits increased to give sufficient margins to cover any DNBR penalties associated with the analysis.

By preventing DNB, adequate heat transfer is provided from the fuel clad to the reactor coolant, thereby preventing clad damage as a result of inadequate cooling. Maximum fuel rod surface temperature is not a design basis, since it is within a few degrees of coolant temperature during operation in the nucleate boiling region. Limits provided by the nuclear control and protection systems are such that this design basis is met for transients associated with Condition II events including overpower transients. There is an additional large DNBR margin at rated power operation and during normal operating transients.

4.4.1.2   Fuel Temperature Design Basis

4.4.1.2.1   Design Basis

During modes of operation associated with Condition I and Condition II events, there is at least a 95-percent probability at a 95-percent confidence level that the peak kW/ft fuel rods will not exceed the uranium dioxide melting temperature. The melting temperature of uranium dioxide is 5080°F (Reference 3) unirradiated and decreasing 58°F per 10,000 MWD/MTU. By precluding uranium dioxide melting, the fuel geometry is preserved and possible adverse effects of molten uranium dioxide on the cladding are eliminated. Design evaluations for Condition I and II events

have shown that fuel melting will not occur for achievable local burnups up to 75,000 MWD/MTU (Reference 81). The NRC has approved design evaluations up to 60,000 MWD/MTU in Reference 81 and up to 62,000 MWD/MTU in Reference 9.

4.4.1.2.2   Discussion

Fuel rod thermal evaluations are performed at rated power, at maximum overpower, and during transients at various burnups. These analyses confirm that this design basis and the fuel integrity design bases given in Section 4.2 are met. They also provide input for the evaluation of Condition III and IV events given in Chapter 15.

The center-line temperature limit has been applied to reload cores with a lead rod average burnup of up to 60,000 MWD/MTU. For higher burnups, the peak kilowatt-per-foot experienced during Condition I and II events is limited to that maximum value which is sufficient to provide that the fuel center-line temperatures remain below the melting temperature for the fuel rods. Thus, the fuel rod design basis that fuel rod damage not occur due to fuel melting continues to be met.

4.4.1.3   Core Flow Design Basis

4.4.1.3.1   Design Basis

Typical minimum value of 94.1 percent of the thermal flow rate is assumed to pass through the fuel rod region of the core and is effective for fuel rod cooling. Coolant flow through the thimble and instrumentation tubes and the leakage between the core barrel and core shroud, head cooling flow, and leakage to the vessel outlet nozzles are not considered effective for heat removal.

4.4.1.3.2   Discussion

Core cooling evaluations are based on the thermal flow rate (minimum flow) entering the reactor vessel. A typical maximum value of 5.9 percent of this value is allotted as bypass flow. This includes rod cluster control guide thimble and instrumentation tube cooling flow, leakage between the core barrel and the core shroud, head cooling flow, and leakage to the vessel outlet nozzles. The shroud core cavity flow is considered as active flow that is effective for fuel rod cooling.

The maximum bypass flow fraction of 5.9 percent assumes the use of thimble plugging devices in the rod cluster control guide thimble tubes that do not contain any other core components.

4.4.1.4   Hydrodynamic Stability Design Basis

Modes of operation associated with Condition I and II events do not lead to hydrodynamic instability.

4.4.1.5   Other Considerations

The design bases described in subsections 4.4.1 through 4.4.1.4 together with the fuel clad and fuel assembly design bases given in subsection 4.2.1 are sufficiently comprehensive that additional limits are not required.

Fuel rod diametral gap characteristics, moderator coolant flow velocity and distribution, and moderator void are not inherently limiting. Each of these parameters is incorporated into the thermal and hydraulic models used to confirm that the above-mentioned design criteria are met. For instance, the fuel rod diametral gap characteristics change with time, as described in subsection 4.2.3, and the fuel rod integrity is evaluated on that basis. The effect of the moderator flow velocity and distribution described in subsection 4.4.2.2 and the moderator void distribution described in subsection 4.4.2.4 are included in the core thermal evaluation and thus affect the design basis.

Meeting the fuel clad integrity criteria covers the possible effects of clad temperature limitations. Clad surface temperature limits are imposed on Condition I and Condition II operation to preclude conditions of accelerated oxidation. A clad temperature limit is applied to the loss-of-coolant accident described in subsection 15.6.5; control rod ejection accident described in subsection 15.4.8; and locked rotor accident described in subsection 15.3.3.

4.4.2 Description of Thermal and Hydraulic Design of the Reactor Core

4.4.2.1 Summary Comparison

Table 4.4-1 provides a comparison of the design parameters for the AP1000, the AP600, and a licensed Westinghouse-designed plant using XL Robust fuel. For the comparison with a plant containing XL Robust fuel, a 193 fuel assembly plant is used, since no domestic Westinghouse designed 157 fuel assembly plants use 17x17 fuel XL Robust fuel.

4.4.2.2 Critical Heat Flux Ratio or DNBR and Mixing Technology

The minimum DNBRs for the rated power and anticipated transient conditions are given in Table 4.4-1. The minimum DNBR in the limiting flow channel is typically downstream of the peak heat flux location (hotspot) due to the increased downstream enthalpy rise.

DNBRs are calculated by using the correlation and definitions described in subsections 4.4.2.2.1 and 4.4.2.2.2. The VIPRE-01 computer code described in subsection 4.4.4.5, is used to determine the flow distribution in the core and the local conditions in the hot channel for use in the DNB correlation. The use of hot channel factors is described in subsections 4.4.4.3.1 (nuclear hot channel factors) and 4.4.2.2.4 (engineering hot channel factors).

4.4.2.2.1 DNB Technology

The primary DNB correlation used for the analysis of the AP1000 fuel is the WRB-2M correlation (Reference 82). The WRB-2M correlation applies to the Robust Fuel Assemblies, which are planned to be used in the AP1000 core. This correlation applies to most AP1000 conditions.

A correlation limit of 1.14 is applicable for the WRB-2M correlation.

The applicable range of parameters for the WRB-2M correlation is:

Pressure $1495 \leq P \leq 2425$ psia
Local mass velocity $0.97 \leq G_{loc}/10^6 \leq 3.1$ lb/ft^2-hr
Local quality $-0.1 \leq X_{loc} \leq 0.29$
Heated length, inlet to CHF location $L_H \leq 14$ feet
Grid spacing $10 \leq g_{sp} \leq 20.6$ inches
Equivalent hydraulic diameter $0.37 \leq D_e \leq 0.46$ inches
Equivalent heated hydraulic diameter $0.46 \leq D_h \leq 0.54$ inches

The WRB-2 (Reference 4) or W-3 (References 5 and 6) correlation is used wherever the WRB-2M correlation is not applicable. The WRB-2 correlation limit is 1.17.

The applicable range of parameters for the WRB-2 correlation is:

Pressure $1440 \leq P \leq 2490$ psia
Local mass velocity $0.9 \leq G_{loc}/10^6 \leq 3.7$ lb/ft^2-hr
Local quality $-0.1 \leq X_{loc} \leq 0.3$
Heat length, inlet to DNB location $L_h \leq 14$ feet
Grid spacing $10 \leq g_{sp} \leq 26$ inches
Equivalent hydraulic diameter $0.37 \leq D_e \leq 0.51$ inches
Equivalent heated hydraulic diameter $0.46 \leq D_h \leq 0.59$ inches

The WRB-2 correlation was developed based on mixing vane data and, therefore, is only applicable in the heated rod spans above the first mixing vane grid.

In the heated region below the first mixing vane grid the W-3 correlation (see References 5 and 6), which does not take credit for mixing vane grids, is used to calculate DNBR values. In addition, the W-3 correlation is applied in the analysis of accident conditions where the system pressure is below the range of the primary correlation. For system pressures in the range of 500 to 1000 psia, the W-3 correlation limit is 1.45 (Reference 7). For system pressures greater than 1000 psia, the W-3 correlation limit is 1.30. The pressures associated with some of the steamline break statepoints are in the range of 300 to 500 psia. Using additional information, the W-3 correlation is shown to be applicable with these pressures and a correlation limit of 1.45.

A cold wall factor, described in WCAP-7695-L (Reference 8), is applied to the W-3 DNB correlation to conservatively account for the presence of the unheated thimble surfaces.

4.4.2.2.2   Definition of DNBR

The DNB heat flux ratio, DNBR, as applied to typical cells (flow cells with all walls heated) and thimble cells (flow cells with heated and unheated walls) is defined as:

$$DNBR = \frac{q"_{DNB,\ predicted}}{q"_{actual}}$$

where:

$$q''_{DNB,\ predicted} = \frac{q''_{WRB-2M}}{F} \text{ or } q''_{DNB,\ predicted} = \frac{q''_{WRB-2}}{F}$$

q''_{WRB-2M} = the uniform DNB heat flux as predicted by the WRB-2M DNB correlation

q''_{WRB-2} = the uniform DNB heat flux as predicted by the WRB-2 DNB correlation

F = the flux shape factor to account for nonuniform axial heat flux distributions (Reference 10) with the term "C" modified as in Reference 5

q''_{actual} = the actual local heat flux

The DNBR as applied to the W-3 DNB correlation is:

$$DNBR = \frac{q''_{predicted}}{q''_{actual}}$$

where:

$$q''_{predicted} = \frac{q''_{EU-W-3}\ x\ CWF}{F}$$

q''_{EU-W-3} = the uniform DNB heat flux as predicted by the W-3 DNB correlation (Reference 5)

$$CWF = 1.0\text{-}Ru\ [T]$$

where:

$$T = 13.76 - 1.372e^{1.78x} - 4.732\ (\frac{G}{10^6})^{-0.0535} - 0.0619\ (\frac{P}{1000})^{0.14} - 8.509\,D_h^{0.017}$$

$Ru = 1\text{-}D_e/D_h$

If the cold wall factor is used (thimble cell), D_h is used in evaluating q''_{EU-W-3}. If the CWF is not used (typical cells), set CWF = 1.0.

4.4.2.2.3   Mixing Technology

The rate of heat exchange by mixing between flow channels is proportional to the difference in the local mean fluid enthalpy of the respective channels, the local fluid density, and the flow velocity. The proportionality is expressed by the dimensionless thermal diffusion coefficient (TDC) which is defined as:

$$\text{TDC} = \frac{w'}{\rho\, V a}$$

where:

w′ = flow exchange rate per unit length (lbm/ft.-s)
ρ = fluid density (lbm/ft.^{3})
V   = fluid velocity (ft./s)
a   = lateral flow area between channels per unit length (ft.^{2}/ft.)

The application of the thermal diffusion coefficient in the VIPRE-01 analysis for determining the overall mixing effect or heat exchange rate is presented in Reference 83.

As discussed in WCAP-7941-P-A (Reference 12) those series of tests, using the "R" mixing vane grid design on 13-, 26-, and 32-inch grid spacing, were conducted in pressurized water loops at Reynolds numbers similar to that of a pressurized water reactor core under the following single- and two-phase (subcooled boiling) flow conditions:

- Pressure   1500 to 2400 psia
- Inlet temperature   332 to 642°F
- Mass velocity   1.0 to 3.5 x 10^6 lbm/hr-ft.^{2}
- Reynolds number   1.34 to 7.45 x 10^5
- Bulk outlet quality   -52.1 to -13.5 percent

The thermal diffusion coefficient is determined by comparing the THINC code predictions with the measured subchannel exit temperatures. Data for 26-inch axial grid spacing are presented in Figure 4.4-1, where the thermal diffusion coefficient is plotted versus the Reynolds number. The thermal diffusion coefficient is found to be independent of the Reynolds number, mass velocity, pressure, and quality over the ranges tested. The two-phase data (local, subcooled boiling) falls within the scatter of the single-phase data. The effect of two-phase flow on the value of the thermal diffusion coefficient is demonstrated in WCAP-7941-P-A (Reference 12), by Rowe and Angle (References 13 and 14), and Gonzalez-Santalo and Griffith (Reference 15). In the subcooled boiling region, the values of the thermal diffusion coefficient are indistinguishable from the single-phase values. In the quality region, Rowe and Angle show that in the case with rod spacing similar to that in pressurized water reactor core geometry, the value of the thermal diffusion coefficient increased with quality to a point and then decreased, but never below the single-phase value. Gonzalez-Santalo and Griffith show that the mixing coefficient increased as the void fraction increased.

The data from these tests on the R-mixing vane grid show that a design thermal diffusion coefficient value of 0.038 (for 26-inch grid spacing) can be used in determining the effect of coolant mixing in the THINC analysis. An equivalent value of the mixing coefficient is used in the VIPRE-01 evaluations (Reference 83). A mixing test program similar to the one just described was conducted for the current 17 x 17 geometry and mixing vane grids on 26-inch spacing, as described in WCAP-8298-P-A (Reference 16). The mean value of the thermal diffusion coefficient obtained from these tests is 0.059.

The inclusion of intermediate flow mixer grids in the upper spans of the fuel assembly results in a grid spacing of approximately 10 inches giving higher values of the thermal diffusion coefficient. A conservative value of the thermal diffusion coefficient, .038, is used to determine the effect of coolant mixing in the core thermal performance analysis.

4.4.2.2.4 Hot Channel Factors

The total hot channel factors for heat flux and enthalpy rise are defined as the maximum-to-core-average ratios of these quantities. The heat flux hot channel factor considers the local maximum linear heat generation rate at a point (the hotspot), and the enthalpy rise hot channel factor involves the maximum integrated value along a channel (the hot channel).

Each of the total hot channel factors is composed of a nuclear hot channel factor, subsection 4.4.4.3, describing the neutron power distribution and an engineering hot channel factor, which allows for variations in flow conditions and fabrication tolerances. The engineering hot channel factors are made up of subfactors which account for the influence of the variations of fuel pellet diameter, density, enrichment, and eccentricity; inlet flow distribution; flow redistribution; and flow mixing.

Heat Flux Engineering Hot Channel Factor, F_Q^E

The heat flux engineering hot channel factor is used to evaluate the maximum linear heat generation rate in the core. This subfactor is determined by statistically combining the fabrication variations for fuel pellet diameter, density, and enrichment. As shown in WCAP-8174 (Reference 17), no DNB penalty need be taken for the short, relatively low-intensity heat flux spikes caused by variations in the above parameters, as well as fuel pellet eccentricity and fuel rod diameter variation.

Enthalpy Rise Engineering Hot Channel Factor, $F_{\Delta H}^E$

The effect of variations in flow conditions and fabrication tolerances on the hot channel enthalpy rise is directly considered in the VIPRE-01 core thermal subchannel analysis, described in subsection 4.4.4.5.1 under any reactor opening condition. The following items are considered as contributors to the enthalpy rise engineering hot channel factor:

- Pellet diameter, density, and enrichment

  Variations in pellet diameter, density, and enrichment are considered statistically in establishing the limit DNBRs, described in subsection 4.4.1.1.2, for the Revised Thermal

Design Procedure (Reference 2). Uncertainties in these variables are determined from sampling of manufacturing data.

- Inlet flow maldistribution

  The consideration of inlet flow maldistribution in core thermal performances is described in subsection 4.4.4.2.2. A design basis of five-percent reduction in coolant flow to the hot assembly is used in the VIPRE-01 analyses.

- Flow redistribution

  The flow redistribution accounts for the reduction in flow in the hot channel resulting from the high flow resistance in the channel due to the local or bulk boiling. The effect of the nonuniform power distribution is inherently considered in the VIPRE-01 analyses for every operating condition evaluated.

- Flow mixing

  The subchannel mixing model incorporated in the VIPRE-01 code and used in reactor design is based on experimental data, as detailed in WCAP-7667-P-A (Reference 18) and discussed in subsections 4.4.2.2.3 and 4.4.4.5.1. The mixing vanes incorporated in the spacer grid design induce additional flow mixing between the various flow channels in a fuel assembly as well as between adjacent assemblies. This mixing reduces the enthalpy rise in the hot channel resulting from local power peaking or unfavorable mechanical tolerances. The VIPRE-01 mixing model is discussed in Reference 83.

4.4.2.2.5 Effects of Rod Bow on DNBR

The phenomenon of fuel rod bowing, as described in WCAP-8691 (Reference 19), is accounted for in the DNBR safety analysis of Condition I and Condition II events for each plant application. Applicable generic credits for margin resulting from retained conservatism in the evaluation of DNBR and/or margin obtained form measured plant operating parameters (such as $F_{\Delta H}^N$ or core flow), which are less limiting than those required by the plant safety analysis, can be used to offset the effect of rod bow.

For the safety analysis of the AP1000, sufficient DNBR margin was maintained, as described in subsection 4.4.1.1.2, to accommodate the full and low flow rod bow DNBR penalties identified in Reference 20. The referenced penalties are applicable to the analyses using the WRB-2M or WRB-2 DNB correlations.

The maximum rod bow penalties (less than about 2 percent DNBR) accounted for in the design safety analysis are based on an assembly average burnup of 24,000 MWD/MTU. At burnups greater than 24,000 MWD/MTU, credit is taken for the effect of $F_{\Delta H}^N$ burndown, due to the decrease in fissionable isotopes and the buildup of fission product inventory, and no additional rod bow penalty is required (Reference 21).

In the upper spans of the fuel assembly, additional restraint is provided with the intermediate flow mixer grids such that the grid-to-grid spacing in those spans with intermediate flow mixer grids is approximately 10 inches compared to approximately 20 inches in the other spans. Using the NRC approved scaling factor [see WCAP 8691 (Reference 19) and Reference 21], results in predicted channel closure in the limiting 10 inch spans of less than 50 percent closure. Therefore, no rod bow DNBR penalty is required in the 10 inch spans in the safety analyses.

4.4.2.3   Linear Heat Generation Rate

The core average and maximum linear heat generation rates are given in Table 4.4-1. The method of determining the maximum linear heat generation rate is given in subsection 4.3.2.2.

4.4.2.4   Void Fraction Distribution

The calculated core average and the hot subchannel maximum and average void fractions are presented in Table 4.4-2 for operation at full power. The void models used in the VIPRE-W code are described in subsection 4.4.2.7.3.

4.4.2.5   Core Coolant Flow Distribution

The VIPRE-01 code is used to calculate the flow and enthalpy distribution in the core for use in safety analysis. Extensive experimental verification of VIPRE-01 is presented in Reference 84.

4.4.2.6   Core Pressure Drops and Hydraulic Loads

4.4.2.6.1   Core Pressure Drops

The analytical model and experimental data used to calculate the pressure drops shown in Table 4.4-1 are described in subsection 4.4.2.7. The core pressure drop includes the fuel assembly, lower core plate, and upper core plate pressure drops. The full-power operation pressure drop values shown in Table 4.4-1 are the unrecoverable pressure drops across the vessel, including the inlet and outlet nozzles, and across the core. These pressure drops are based on the best-estimate flow for actual plant operating conditions as described in subsection 5.1.4. This subsection also defines and describes the thermal design flow (minimum flow) that is the basis for reactor core thermal performance and the mechanical design flow (maximum flow) that is used in the mechanical design of the reactor vessel internals and fuel assemblies. Since the best-estimate flow is that flow which is most likely to exist in an operating plant, the calculated core pressure drops in Table 4.4-1 are based on this best-estimate flow rather than the thermal design flow.

The uncertainties associated with the core pressure drop values are presented in subsection 4.4.2.9.2.

4.4.2.6.2   Hydraulic Loads

Figure 4.2-2 shows the fuel assembly hold-down springs. These springs are designed to keep the fuel assemblies in contact with the lower core plate under Condition I and II events, except for the turbine overspeed transient associated with a loss of external load. The hold-down springs are designed to tolerate the possibility of an overdeflection associated with fuel assembly lift-off for this case and to provide contact between the fuel assembly and the lower core plate following this

transient. More adverse flow conditions occur during a loss-of-coolant accident. These conditions are presented in subsection 15.6.5.

Hydraulic loads at normal operating conditions are calculated considering the best-estimate flow, described in Section 5.1, and accounting for the minimum core bypass flow based on manufacturing tolerances. Core hydraulic loads at cold plant startup conditions are based on the cold best-estimate flow, but are adjusted to account for the coolant density difference. Conservative core hydraulic loads for a pump overspeed transient, which could possibly create a flow rate 18-percent greater than the best estimate flow, are evaluated to be approximately twice the fuel assembly weight.

Hydraulic verification tests for the fuel assembly are described in Reference 86.

4.4.2.7 Correlation and Physical Data

4.4.2.7.1 Surface Heat Transfer Coefficients

Forced convection heat transfer coefficients are obtained from the Dittus-Boelter correlation (Reference 24), with the properties evaluated at bulk fluid conditions:

$$\frac{hD_c}{K} = 0.023 \frac{D_c G^{0.9}}{\mu} \frac{C_\rho \mu^{0.4}}{K}$$

where:

- h = heat transfer coefficient (btu/h-ft^2-°F)
- D_e = equivalent diameter (ft)
- K = thermal conductivity (Btu/h-ft-°F)
- G = mass velocity (lbm/h-ft^2)
- μ = dynamic viscosity (lbm/ft-h)
- C_p = heat capacity (Btu/lb-°F)

This correlation has been shown to be conservative (Reference 25) for rod bundle geometries with pitch-to-diameter ratios in the range used by pressurized water reactors.

The onset of nucleate boiling occurs when the clad wall temperature reaches the amount of superheat predicted by Thom's correlation (Reference 26). After this occurrence, the outer clad wall temperature is determined by:

$$\Delta T_{sat} = [0.072 \exp(-P/1260)](q'')^{0.5}$$

where:

- ΔT_{sat} = wall superheat, $T_W - T_{sat}$ (°F)
- q'' = wall heat flux (Btu/h-ft^2)
- P = pressure (psia)
- T_w = outer clad wall temperature (°F)
- T_{sat} = saturation temperature of coolant at pressure P (°F)

4.4.2.7.2   Total Core and Vessel Pressure Drop

Unrecoverable pressure losses occur as a result of viscous drag (friction) and/or geometry changes (form) in the fluid flow path. The flow field is assumed to be incompressible, turbulent, single-phase water. Those assumptions apply to the core and vessel pressure drop calculations for the purpose of establishing the primary loop flow rate. Two-phase considerations are neglected in the vessel pressure drop evaluation because the core average void is negligible, as shown in Table 4.4-2. Two-phase flow considerations in the core thermal subchannel analysis are considered and the models are described in subsection 4.4.4.2.3. Core and vessel pressure losses are calculated by equations of the form:

$$\Delta P_L = (K + f \frac{L}{D_c}) \frac{\rho V^2}{2 g_c (144)}$$

where:

ΔP_L = unrecoverable pressure drop (lb/in.^{2})
ρ = fluid density (lbm/ft^3)
L = length (ft)
D_e = equivalent diameter (ft)
V = fluid velocity (ft/s)
g_c = 32.174 (lbm-ft/lb p-s^2)
K = form loss coefficient (dimensionless)
f = friction loss coefficient (dimensionless)

Fluid density is assumed to be constant at the appropriate value for each component in the core and vessel. Because of the complex core and vessel flow geometry, precise analytical values for the form and friction loss coefficients are not available. Therefore, experimental values for these coefficients are obtained from geometrically similar models.

Values are quoted in Table 4.4-1 for unrecoverable pressure loss across the reactor vessel, including the inlet and outlet nozzles, and across the core. The results of full-scale tests of core components and fuel assemblies are used in developing the core pressure loss characteristic.

Tests of the primary coolant loop flow rates are made prior to initial criticality as described in subsection 4.4.5.1, to verify that the flow rates used in the design, which are determined in part from the pressure losses calculated by the method described here, are conservative. See Section 14.2 for preoperational testing.

4.4.2.7.3   Void Fraction Correlation

VIPRE-01 considers two-phase flow in two steps. First, a quality model is used to compute the flowing vapor mass fraction (true quality) including the effects of subcooled boiling. Then, given the true void quality, a bulk void model is applied to compute the vapor volume fraction (void fraction).

VIPRE-01 uses a profile fit model (Reference 83) for determining subcooled quality. It calculates the local vapor volumetric fraction in forced convection boiling by: 1) predicting the point of bubble departure from the heated surface and 2) postulating a relationship between the true local vapor fraction and the corresponding thermal equilibrium value.

The void fraction in the bulk boiling region is predicted by using homogeneous flow theory and assuming no slip. The void fraction in this region is therefore a function only of the thermodynamic quality.

4.4.2.8   Thermal Effects of Operational Transients

DNB core safety limits are generated as a function of coolant temperature, pressure, core power, and axial power imbalance. Steady-state operation within these safety limits provides that the DNB design basis is met. Subsection 15.0.6 discusses the overtemperature ΔT trip (based on DNBR limit) versus T_{avg}. This system provides protection against anticipated operational transients that are slow with respect to fluid transport delays in the primary system. In addition, for fast transients (such as uncontrolled rod bank withdrawal at power incident as described in subsection 15.4.2, specific protection functions are provided as described in Section 7.2. The use of these protection functions is described in Chapter 15.

4.4.2.9   Uncertainties in Estimates

4.4.2.9.1   Uncertainties in Fuel and Clad Temperatures

As described in subsection 4.4.2.11, the fuel temperature is a function of crud, oxide, clad, pellet-clad gap, and pellet conductances. Uncertainties in the fuel temperature calculation are essentially of two types: fabrication uncertainties, such as variations in the pellet and clad dimensions and the pellet density; and model uncertainties, such as variations in the pellet conductivity and the gap conductance. These uncertainties have been quantified by comparison of the thermal model to the in-pile thermocouple measurements (References 30 through 36), by out-of-pile measurements of the fuel and clad properties (References 37 through 48), and by measurements of the fuel and clad dimensions during fabrication. The resulting uncertainties are then used in the evaluations involving the fuel temperature. The effect of densification on fuel temperature uncertainties is also included in the calculation of the total uncertainty.

In addition to the temperature uncertainty described above, the measurement uncertainty in determining the local power and the effect of density and enrichment variations on the local power are considered in establishing the heat flux hot channel factor. These uncertainties are described in subsection 4.3.2.2.1.

Reactor trip setpoints, as specified in the technical specifications, include allowance for instrument and measurement uncertainties such as calorimetric error, instrument drift and channel reproducibility, temperature measurement uncertainties, noise, and heat capacity variations.

Uncertainty in determining the cladding temperature results from uncertainties in the crud and oxide thicknesses. Because of the excellent heat transfer between the surface of the rod and the coolant, the film temperature drop does not appreciably contribute to the uncertainty.

4.4.2.9.2   Uncertainties in Pressure Drops

Core and vessel pressure drops based on the best-estimate flow, as described in Section 5.1, are quoted in Table 4.4-1. The uncertainties quoted are based on the uncertainties in both the test results and the analytical extension of these values to the reactor application.

A major use of the core and vessel pressure drops is to determine the primary system coolant flow rates, as described in Section 5.1. In addition, as described in subsection 4.4.5.1, tests on primary system prior to initial criticality, are conducted to verify that a conservative primary system coolant flow rate has been used in the design and analysis of the plant.

4.4.2.9.3   Uncertainties Due to Inlet Flow Maldistribution

The effects of uncertainties in the inlet flow maldistribution criteria used in the core thermal analyses are described in subsection 4.4.4.2.2.

4.4.2.9.4   Uncertainty in DNB Correlation

The uncertainty in the DNB correlation described in subsection 4.4.2.2, is written as a statement on the probability of not being in DNB based on the statistics of the DNB data. This is described in subsection 4.4.2.2.2.

4.4.2.9.5   Uncertainties in DNBR Calculations

The uncertainties in the DNBRs calculated by the VIPRE-01 analyses, discussed in subsection 4.4.4.5.1, due to uncertainties in the nuclear peaking factors are accounted for by applying conservatively high values of the nuclear peaking factors. Measurement error allowances are included in the statistical evaluation of the limit DNBR described in subsection 4.4.1.1 using the Revised Thermal Design Procedure. More information is provided in WCAP-11397-P-A (Reference 2). In addition, conservative values for the engineering hot channel factors are used as presented in subsection 4.4.2.2.4. The results of a sensitivity study, WCAP-8054-P-A (Reference 22), with THINC-IV, a VIPRE-01 equivalent code, show that the minimum DNBR in the hot channel is relatively insensitive to variations in the core-wide radial power distribution (for the same value of $F_{\Delta H}^{N}$).

The ability of the VIPRE-01 computer code to accurately predict flow and enthalpy distributions in rod bundles is discussed in subsection 4.4.4.5.1 and in Reference 83. Studies (Reference 84) have been performed to determine the sensitivity of the minimum DNBR to the void fraction correlation (see also subsection 4.4.2.7.3) and the inlet flow distributions. The results of these studies show that the minimum DNBR is relatively insensitive to variation in these parameters. Furthermore, the VIPRE-01 flow field model for predicting conditions in the hot channels is consistent with that used in the derivation of the DNB correlation limits including void/quality modeling, turbulent mixing and crossflow and two phase flow (Reference 83).

4.4.2.9.6   Uncertainties in Flow Rates

The uncertainties associated with reactor coolant loop flow rates are discussed in Section 5.1. A thermal design flow is defined for use in core thermal performance evaluations accounting for both prediction and measurement uncertainties. In addition, another 5.9 percent of the thermal design flow is assumed to be ineffective for core heat removal capability because it bypasses the core through the various available vessel flow paths described in subsection 4.4.4.2.1.

4.4.2.9.7   Uncertainties in Hydraulic Loads

As described in subsection 4.4.2.6.2, hydraulic loads on the fuel assembly are evaluated for a pump overspeed transient which creates flow rates 18 percent greater than the best estimate flow. The best estimate flow is the most likely flow rate value for the actual plant operating condition.

4.4.2.9.8   Uncertainty in Mixing Coefficient

A conservative value of the mixing coefficient, that is, the thermal diffusion coefficient, is used in the VIPRE-01 analyses.

4.4.2.10   Flux Tilt Considerations

Significant quadrant power tilts are not anticipated during normal operation since this phenomenon is caused by some asymmetric perturbation. A dropped or misaligned rod cluster control assembly could cause changes in hot channel factors. These events are analyzed separately in Chapter 15.

Other possible causes for quadrant power tilts include X-Y xenon transients, inlet temperature mismatches, enrichment variations within tolerances, and so forth.

In addition to unanticipated quadrant power tilts as described above, other readily explainable asymmetries may be observed during calibration of the ex-core detector quadrant power tilt alarm. During operation, in-core maps are taken at least one per month and additional maps are obtained periodically for calibration purposes. Each of these maps is reviewed for deviations from the expected power distributions.

Asymmetry in the core, from quadrant to quadrant, is frequently a consequence of the design when assembly and/or component shuffling and rotation requirements do not allow exact symmetry preservation. In each case, the acceptability of an observed asymmetry, planned or otherwise, depends solely on meeting the required accident analyses assumptions. In practice, once acceptability has been established by review of the incore maps, the quadrant power tilt alarms and related instrumentation are adjusted to indicate zero quadrant power tilt ratio as the final step in the calibration process. This action confirms that the instrumentation is correctly calibrated to alarm in the event an unexplained or unanticipated change occurs in the quadrant-to-quadrant relationships between calibration intervals.

Proper functioning of the quadrant power tilt alarm is significant. No allowances are made in the design for increased hot channel factors due to unexpected developing flux tilts, since likely causes are presented by design or procedures or are specifically analyzed.

Finally, in the event that unexplained flux tilts do occur, the Technical Specifications provide appropriate corrective actions to provide continued safe operation of the reactor.

4.4.2.11   Fuel and Cladding Temperatures

Consistent with the thermal-hydraulic design bases described in subsection 4.4.1, the following discussion pertains mainly to fuel pellet temperature evaluation. A description of fuel clad integrity is presented in subsection 4.2.3.1.

The thermal-hydraulic design provides that the maximum fuel temperature is below the melting point of uranium dioxide, subsection 4.4.1.2. To preclude center melting and to serve as a basis for overpower protection system setpoints, a calculated center-line fuel temperature of 4700°F is selected as the overpower limit. This provides sufficient margin for uncertainties in the thermal evaluations, as described in subsection 4.4.2.9.1. The temperature distribution within the fuel pellet is predominantly a function of the local power density and the uranium dioxide thermal conductivity. However, the computation of radial fuel temperature distributions combines crud, oxide, clad gap, and pellet conductances. The factors which influence these conductances, such as gap size (or contact pressure), internal gas pressure, gas composition, pellet density, and radial power distribution within the pellet, have been combined into a semi-empirical thermal model, discussed in subsection 4.2.3.3, that includes a model for time-dependent fuel densification, as given in WCAP-10851-P-A (Reference 49) and WCAP-15063-P-A, Revision 1 (Reference 85). This thermal model enables the determination of these factors and their net effects on temperature profiles. The temperature predictions have been compared to in-pile fuel temperature measurements (References 30 through 36, 50 and 85) and melt radius data (References 51 and 52) with good results.

Fuel rod thermal evaluations (fuel centerline, average and surface temperatures) are performed at several times in the fuel rod lifetime (with consideration of time-dependent densification) to determine the maximum fuel temperatures.

The principal factors employed in the determination of the fuel temperature follow.

4.4.2.11.1   Uranium Dioxide Thermal Conductivity

The thermal conductivity of uranium dioxide was evaluated from data reported in References 37 through 48 and 53. At the higher temperatures, thermal conductivity is best obtained by using the integral conductivity to melt. From an examination of the data, it has been concluded that the best estimate is:

$$\int_{o}^{2800} K dt = 93 \, \text{W/cm}$$

This conclusion is based on the integral values reported in References 51 and 53 through 57.

The design curve for the thermal conductivity is shown in Figure 4.4-2. The section of the curve at temperatures between 0° and 1300°C is in agreement with the recommendation of the

International Atomic Energy Agency (IAEA) panel (Reference 58). The section of the curve above 1300°C is derived for an integral value of 93 W/cm. (References 51, 53, and 57).

Thermal conductivity for uranium dioxide at 95-percent theoretical density can be represented by the following equation:

$$K = \frac{1}{11.8 + 0.0238\,T} + 8.775 \times 10^{-13}\,T^3$$

where:

K = W/cm-°C
T = °C.

4.4.2.11.2 Radial Power Distribution in Uranium Dioxide Fuel Rods

An accurate description of the radial power distribution as a function of burnup is needed for determining the power level for incipient fuel melting and other important performance parameters, such as pellet thermal expansion, fuel swelling, and fission gas release rates. Radial power distribution in uranium dioxide fuel rods is determined with the neutron transport theory code, LASER. The LASER code has been validated by comparing the code predictions on radial burnup and isotopic distributions with measured radial microdrill data, as detailed in WCAP-6069 (Reference 59) and WCAP-3385-56 (Reference 60). A radial power depression factor, f, is determined using radial power distributions predicted by LASER. The factor, f, enters into the determination of the pellet centerline temperature, T_c, relative to the pellet surface temperature, T_g, through the expression:

$$\int_{T_i}^{T_c} K(T)\,dT = \frac{q''f}{4\pi}$$

where:

K(T) = the thermal conductivity for uranium dioxide with a uniform density distribution
q″ = the linear power generation rate

4.4.2.11.3 Gap Conductance

The temperature drop across the pellet-clad gap is a function of the gap size and the thermal conductivity of the gas in the gap. The gap conductance model is selected so that when combined with the uranium dioxide thermal conductivity model, the calculated fuel center-line temperature reflect the in-pile temperature measurements. A more detailed description of the gap conductance model is presented in WCAP-10851-P-A (Reference 49) and WCAP-15063-P-A (Reference 85).

4.4.2.11.4 Surface Heat Transfer Coefficients

The fuel rod surface heat transfer coefficients during subcooled forced convection and nucleate boiling are presented in subsection 4.4.2.7.1.

4.4.2.11.5 Fuel Clad Temperatures

The outer surface of the fuel rod at the hotspot operates at a temperature a few degrees above fluid temperature for steady-state operation at rated power throughout core life due to the onset of nucleate boiling. At beginning of life this temperature is the same as the clad metal outer surface.

During operation over the life of the core, the buildup of oxides and crud on the fuel rod surface causes the clad surface temperature to increase. Allowance is made in the fuel center melt evaluation for this temperature rise. Since the thermal-hydraulic design basis limits DNB, adequate heat transfer is provided between the fuel clad and the reactor coolant so that the core thermal output is not limited by considerations of clad temperature.

4.4.2.11.6 Treatment of Peaking Factors

The total heat flux hot channel factor, F_Q, is defined by the ratio of the maximum-to-core-average heat flux. The design value of F_Q, as presented in Table 4.3-2 and described in subsection 4.3.2.2.6, is 2.6 for normal operation.

As described in subsection 4.3.2.2.6, the peak linear power resulting from overpower transients/operator errors (assuming a maximum overpower of 118 percent) is less than 22.45 kW/ft. The centerline fuel temperature must be below the uranium dioxide melt temperature over the lifetime of the rod, including allowances for uncertainties. The fuel temperature design basis is described in subsection 4.4.1.2 and results in a maximum allowable calculated center-line temperature of 4700°F. The peak linear power for prevention of center-line melt is 22.5 kW/ft. The center-line temperature at the peak linear power resulting from overpower transients/operator errors (assuming a maximum overpower of 118 percent) is below that required to produce melting.

4.4.3 Description of the Thermal and Hydraulic Design of the Reactor Coolant System

4.4.3.1 Plant Configuration Data

Plant configuration data for the thermal-hydraulic and fluid systems external to the core are provided as appropriate in Chapters 5, 6, and 9. Areas of interest are as follows:

- Total coolant flow rates for the reactor coolant system and each loop are provided in Table 5.1-3. Flow rates employed in the evaluation of the core are presented throughout Section 4.4.

- Total reactor coolant system volume including pressurizer and surge line and reactor coolant system liquid volume, including pressurizer water at steady-state power conditions, are given in Table 5.1-2.

- The flow path length through each volume may be calculated from physical data provided in Table 5.1-2.

- Line lengths and sizes for the passive core cooling system are determined to provide a total system resistance which will provide, as a minimum, the fluid delivery rates assumed in the safety analyses described in Chapter 15.

- The parameters for components of the reactor coolant system are presented in Section 5.4.

- The steady-state pressure drops and temperature distributions through the reactor coolant system are presented in Table 5.1-1.

4.4.3.2   Operating Restrictions on Pumps

The minimum net positive suction head is established before operating the reactor coolant pumps. The operator verifies that the system pressure satisfies net positive suction head requirements prior to operating the pumps.

4.4.3.3   Power-Flow Operating Map (Boiling Water Reactor BWR])

This subsection is not applicable to AP1000.

4.4.3.4   Temperature-Power Operating Map (PWR)

The relationship between reactor coolant system temperature and power is a linear relationship between zero and 100-percent power.

The effects of reduced core flow due to inoperative pumps is described in subsections 5.4.1 and 15.2.6 and Section 15.3. The AP1000 does not include power operation with one pump out of service. Natural circulation capability of the system is described in subsection 5.4.2.3.2.

4.4.3.5   Load Following Characteristics

Load follow using control rod and gray rod motion is described in subsection 4.3.2.4.16. The reactor power is controlled to maintain average coolant temperature at a value which is a linear function of load, as described in Section 7.7.

4.4.3.6   Thermal and Hydraulic Characteristics Summary Table

The thermal and hydraulic characteristics are given in Tables 4.1-1, 4.4-1, and 4.4-2.

4.4.4   Evaluation

4.4.4.1   Critical Heat Flux

The critical heat flux correlations used in the core thermal analysis are explained in subsection 4.4.2.

4.4.4.2   Core Hydraulics

4.4.4.2.1   Flow Paths Considered in Core Pressure Drop and Thermal Design

The following flow paths for core bypass are considered:

A.   Flow through the spray nozzles into the upper head for head cooling purposes

B.   Flow entering into the rod cluster control and gray rod cluster guide thimbles

C.   Leakage flow from the vessel inlet nozzle directly to the vessel outlet nozzle through the gap between the vessel and the barrel

D.   Flow introduced through the core shroud for the purpose of cooling and not considered available for core cooling

The above contributions are evaluated to confirm that the design value of the core bypass flow is met.

Of the total allowance, one part is associated with the core and the remainder is associated with the internals (items A, C, and D above). Calculations have been performed using drawing tolerances in the worst direction and accounting for uncertainties in pressure losses. Based on these calculations, the core bypass is no greater than the 5.9 percent design value.

Flow model test results for the flow path through the reactor are described in subsection 4.4.2.7.2.

4.4.4.2.2   Inlet Flow Distributions

A core inlet flow distribution reduction of five percent to the hot assembly inlet is used in the VIPRE-01 analyses of DNBR in the AP1000 core. Studies shown in WCAP-8054-P-A (Reference 22), made with THINC-IV, a VIPRE-01 equivalent code, show that flow distributions significantly more nonuniform than five percent have a very small effect on DNBR, which is accounted for in the DNB analysis.

4.4.4.2.3   Empirical Friction Factor Correlations

The friction factor for VIPRE-01 in the axial direction, parallel to the fuel rod axis, is evaluated using a correlation for a smooth tube (Reference 83). The effect of two-phase flow on the friction loss is expressed in terms of the single-phase friction pressure drop and a two-phase friction multiplier. The multiplier is calculated using the homogenous equilibrium flow model.

The flow in the lateral directions, normal to the fuel rod axis, views the reactor core as a large tube bank. Thus, the lateral friction factor proposed by Idel'chik (Reference 64) is applicable. This correlation is of the form:

$$F_L = A \, Re_L^{-0.2}$$

where:

A   =   a function of the rod pitch and diameter as given in Idel'chik (Reference 64)

Re_L =   the lateral Reynolds number based on the rod diameter

The comparisons of predictions to data given in Reference 83 verify the applicability of the VIPRE-01 correlations in PWR design.

4.4.4.3   Influence of Power Distribution

The core power distribution, which is largely established at beginning of life by fuel enrichment, loading pattern, and core power level, is also a function of variables such as control rod worth and position, and fuel depletion through lifetime. Radial power distributions in various planes of the core are often illustrated for general interest. However, the core radial enthalpy rise distribution, as determined by the integral of power up each channel, is of greater importance for DNBR analyses. These radial power distributions, characterized by $F_N^{\Delta H}$ (defined in subsection 4.3.2.2.1), as well as axial heat flux profiles are discussed in the subsections 4.4.4.3.1 and 4.4.4.3.2.

4.4.4.3.1   Nuclear Enthalpy Rise Hot Channel Factor, $F_{\Delta H}^N$

Given the local power density q′ (kW/ft) at a point x, y, z in a core with N fuel rods and height H, then:

$$F_{\Delta H}^N = \frac{\text{hot rod power}}{\text{average rod power}} = \frac{\text{Max} \int_o^H q' x_o\, y_o, z_o)\, dz}{\dfrac{1}{N} \sum_{\text{all rods}} \int_o^H q'(x, y, z)\, dz}$$

The way in which $F_{\Delta H}^N$ is used in the DNBR calculation is important. The location of minimum DNBR depends on the axial profile, and the value of DNBR depends on the enthalpy rise to that point. Basically, the maximum value of the rod integral power is used to identify the most likely rod for minimum DNBR. An axial power profile is obtained that, when normalized to the design value of $F_{\Delta H}^N$, recreates the axial heat flux along the limiting rod. The surrounding rods are assumed to have the same axial profile with rod average powers which are typical distributions found in hot assemblies. In this manner, worst-case axial profiles can be combined with worst-case radial distributions for reference DNBR calculations.

It should be noted again that $F_{\Delta H}^N$ is an integral and is used as such in DNBR calculations. Local heat fluxes are obtained by using hot channel and adjacent channel explicit power shapes which take into account variations in horizontal power shapes throughout the core.

For operation at a fraction of full power, the design $F_{\Delta H}^N$ used is given by:

$$F_{\Delta H}^N = F_{\Delta H}^{RTP}\,[1 + 0.3(1 - P)]$$

where:

$F_{\Delta H}^N$ is the limit at rated thermal power (RTP):

P is the fraction of rated thermal power and $F_{\Delta H}^{RTP}$ = 1.59.

The permitted relaxation of $F_{\Delta H}^N$ is included in the DNB protection setpoints and allows radial power shape changes with rod insertion to the insertion limits, as detailed in WCAP-7912-P-A (Reference 65). This allows greater flexibility in the nuclear design.

4.4.4.3.2   Axial Heat Flux Distributions

As described in subsection 4.3.2.2, the axial heat flux distribution can vary as a result of rod motion or power change or as a result of a spatial xenon transient which may occur in the axial direction. The ex-core nuclear detectors, as described in subsection 4.3.2.2.7, are used to measure the axial power imbalance. The information from the ex-core detectors is used to protect the core from excessive axial power imbalance. The reference axial shape used in establishing core DNB limits (that is, overtemperature ΔT protection system setpoints) is a chopped cosine with a peak-to-average value of 1.61. The reactor trip system provides automatic reduction of the trip setpoints on excessive axial power imbalance. To determine the magnitude of the setpoint reduction, the reference shape is supplemented by other axial shapes skewed to the bottom and top of the core.

The course of those accidents in which DNB is a concern is analyzed in Chapter 15 assuming that the protection setpoints have been set on the basis of these shapes. In many cases, the axial power distribution in the hot channel changes throughout the course of the accident due to rod motion, coolant temperature, and power level changes.

The initial conditions for the accidents for which DNB protection is required are assumed to be those permissible within the specified axial offset control limits described in subsection 4.3.2.2. In the case of the loss-of-flow accident, the hot channel heat flux profile is very similar to the power density profile in normal operation preceding the accident. It is therefore possible to illustrate the calculated minimum DNBR for conditions representative of the loss-of-flow accident as a function of the flux difference initially in the core. The power shapes are evaluated with a full-power radial peaking factor ($F_{\Delta H}^N$) of 1.59. The radial contribution to the hot rod power shape is conservative both for the initial condition and for the condition at the time of minimum DNBR during the loss-of-flow transient. The minimum DNBR is calculated for the design power shape for non-overpower/overtemperature DNB events. This design shape results in calculated DNBR that bounds the normal operation shapes.

4.4.4.4 Core Thermal Response

A general summary of the steady-state thermal-hydraulic design parameters including thermal output and flow rates is provided in Table 4.4-1.

As stated in subsection 4.4.1, the design bases of the application are to prevent DNB and to prevent fuel melting for Condition I and II events. The protective systems described in Chapter 7 are designed to meet these bases. The response of the core to Condition II transients is given in Chapter 15.

4.4.4.5 Analytical Methods

4.4.4.5.1 Core Analysis

The objective of reactor core thermal design is to determine the maximum heat removal capability in all flow subchannels and to show that the core safety limits, as presented in the technical specifications, are not exceeded while combining engineering and nuclear effects. The thermal design takes into account local variations in dimensions, power generation, flow redistribution, and mixing. The Westinghouse version of VIPRE-01, a three-dimensional subchannel code that has been developed to account for hydraulic and nuclear effects on the enthalpy rise in the core and hot channels, is described in Reference 83, VIPRE-01 modeling of a PWR core is based on a one-pass modeling approach (Reference 83). In the one-pass modeling, hot channels and their adjacent channels are modeled in detail, while the rest of the core is modeled simultaneously on a relatively coarse mesh. The behavior of the hot assembly is determined by superimposing the power distribution upon the inlet flow distribution while allowing for flow mixing and flow distribution between flow channels. Local variations in fuel rod power, fuel rod and pellet fabrication, and turbulent mixing are also considered in determining conditions in the hot channels. Conservation equations of mass, axial and lateral momentum, and energy are solved for the fluid enthalpy, axial flow rate, lateral flow, and pressure drop.

4.4.4.5.2 Steady State Analysis

The VIPRE-01 core model as approved by the NRC (Reference 83) is used with the applicable DNB correlations to determine DNBR distributions along the hot channels of the reactor core under all expected operating conditions. The VIPRE-01 code is described in detail in Reference 84, including discussions on code validation with experimental data. The VIPRE-01 modeling method is described in Reference 83, including empirical models and correlations used. The effect of crud on the flow and enthalpy distribution in the core is not directly accounted for in the VIPRE-01 evaluations. However, conservative treatment by the Westinghouse VIPRE-01 modeling method has been demonstrated to bound this effect in DNBR calculations (Reference 83).

Estimates of uncertainties are discussed in subsection 4.4.2.9.

4.4.4.5.3 Experimental Verification

Extensive additional experimental verification of VIPRE-01 is presented in Reference 84.

The VIPRE-01 analysis is based on a knowledge and understanding of the heat transfer and hydrodynamic behavior of the coolant flow and the mechanical characteristics of the fuel elements. The use of the VIPRE-01 analysis provides a realistic evaluation of the core performance and is used in the thermal hydraulic analyses as described above.

4.4.4.5.4 Transient Analysis

VIPRE-01 is capable of transient DNB analysis. The conservation equations in the VIPRE-01 code contain the necessary accumulation terms for transient calculations. The input description can include one or more of the following time dependent arrays:

1. Inlet flow variation
2. Core heat flux variation
3. Core pressure variation
4. Inlet temperature or enthalpy variation

At the beginning of the transient, the calculation procedure is carried out as in the steady state analysis. The time is incremented by an amount determined either by the user of by the time step control options in the code itself. At each new time step the calculations are carried out with the addition of the accumulation terms which are evaluated using the information from the previous time step. This procedure is continued until a preset maximum time is reached.

At time intervals selected by the user, a complete description of the coolant parameter distributions as well as DNBR is printed out. In this manner the variation of any parameter with time can be readily determined.

4.4.4.6 Hydrodynamic and Flow Power Coupled Instability

Boiling flow may be susceptible to thermohydrodynamic instabilities (Reference 68). These instabilities are undesirable in reactors, since they may cause a change in thermohydraulic conditions that may lead to a reduction in the DNB heat flux relative to that observed during a steady flow condition or to undesired forced vibrations of core components. Therefore, a thermo-hydraulic design criterion was developed which states that modes of operation under Condition I and II events shall not lead to thermohydrodynamic instabilities.

Two specific types of flow instabilities are considered for AP1000 operation. These are the Ledinegg (or flow excursion) type of static instability and the density wave type of dynamic instability.

A Ledinegg instability involves a sudden change in flow rate from one steady state to another. This instability occurs (Reference 68) when the scope of the reactor coolant system pressure drop-flow rate curve:

$$\left(\frac{\partial \Delta P}{\partial G} \,|\, \text{internal} \right)$$

becomes algebraically smaller than the loop supply (pump head) pressure drop-flow rate curve:

$$\left(\frac{\partial \Delta P}{\partial G} \,|\, \text{external} \right)$$

The criterion for stability is thus:

$$\left(\frac{\partial \Delta P}{\partial G} \,|\, \text{internal} \geq \frac{\partial \Delta P}{\partial G} \,|\, \text{external} \right)$$

The reactor coolant pump head curve has a negative slope ($\partial \Delta P/\partial G$ external less than zero), whereas the reactor coolant system pressure drop-flow curve has a positive slope ($\partial \Delta P/\partial G$ internal greater than zero) over the Condition I and Condition II operational ranges. Thus, the Ledinegg instability does not occur.

The mechanism of density wave oscillations in a heated channel has been described by R. T. Lahey and F. J. Moody (Reference 69). Briefly, an inlet flow fluctuation produces an enthalpy perturbation. This perturbs the length and the pressure drop of the single-phase region and causes quality or void perturbations in the two-phase regions that travel up the channel with the flow. The quality and length perturbations in the two-phase region create two-phase pressure drop perturbations. However, since the total pressure drop across the core is maintained by the characteristics of the fluid system external to the core, then the two-phase pressure drop perturbation feeds back to the single-phase region. These resulting perturbations can be either attenuated or self-sustained.

A simple method has been developed by M. Ishii (Reference 70) for parallel closed-channel systems to evaluate whether a given condition is stable with respect to the density wave type of dynamic instability. This method had been used to assess the stability of typical Westinghouse reactor designs, including the design outlined in References 71, 72, and 73, under Condition I and II operation. The results indicate that a large margin-to-density wave instability exists. Increases on the order of 150 percent of rated reactor power would be required for the predicted inception of this type of instability.

The application of the Ishii method (Reference 70) to Westinghouse reactor designs is conservative due to the parallel open-channel feature of Westinghouse pressurized water reactor cores. For such cores, there is little resistance to lateral flow leaving the flow channels of high-power density. There is also energy transfer from channels of high-power density to lower power density channels. This coupling with cooler channels leads to the conclusion that an open-channel

configuration is more stable than the above closed-channel analysis under the same boundary conditions.

Flow stability tests (Reference 74) have been conducted where the closed channel systems were shown to be less stable than when the same channels were cross-connected at several locations. The cross-connections were such that the resistance to channel cross-flow and enthalpy perturbations would be greater than would exist in a pressurized water reactor core which has a relatively low resistance to cross-flow.

Flow instabilities that have been observed have occurred almost exclusively in closed-channel systems operating at low pressures relative to the Westinghouse pressurized water reactor operating pressures. H. S. Kao, T. D. Morgan, and W. B. Parker (Reference 75) analyzed parallel closed-channel stability experiments simulating a reactor core flow. These experiments were conducted at pressures up to 2200 psia. The results showed that, for flow and power levels typical of power reactor conditions, no flow oscillations could be induced above 1200 psia.

Additional evidence that flow instabilities do not adversely affect thermal margin is provided by the data from the rod bundle DNB tests. Many Westinghouse rod bundles have been tested over wide ranges of operating conditions with no evidence of premature DNB or inconsistent data which might be indicative of flow instabilities in the rod bundle.

In summary, it is concluded that thermohydrodynamic instabilities will not occur under Condition I and II for Westinghouse pressurized water reactor designs. A large power margin, greater than 150 percent of rated power, exists to predicted inception of such instabilities. Analysis has been performed which shows that minor plant-to-plant differences in Westinghouse reactor designs such as fuel assembly arrays, power-to-flow ratios, and fuel assembly length do not result in gross deterioration of the above power margins.

4.4.4.7   Fuel Rod Behavior Effects from Coolant Flow Blockage

Coolant flow blockages can occur within the coolant channels of a fuel assembly or external to the reactor core. The effects of fuel assembly blockage within the assembly on fuel rod behavior are more pronounced than external blockages of the same magnitude. In both cases, the flow blockages cause local reductions in coolant flow. The amount of local flow reduction, where the reduction occurs in the reactor, and how far along the flow stream the reduction persists are considerations which will influence the fuel rod behavior. The effects of coolant flow blockages in terms of maintaining rated core performance are determined both by analytical and experimental methods. The experimental data are usually used to augment analytical tools such as computer programs similar to the VIPRE-01 program. Inspection of the DNB correlation (subsection 4.4.2.2 and References 4, 5, and 6) shows that the predicted DNBR is dependent upon the local values of quality and mass velocity.

The VIPRE-01 code is capable of predicting the effects of local flow blockages on DNBR within the fuel assembly on a subchannel basis, regardless of where the flow blockage occurs. Reference 84 shows that, for a fuel assembly similar to the Westinghouse design, VIPRE-01 accurately predicts the flow distribution within the fuel assembly when the inlet nozzle is completely blocked. Full recovery of the flow was found to occur about 30 inches downstream of

the blockage. With the reactor operating at the nominal full-power conditions specified in Table 4.4-1, the effects of an increase in enthalpy and decrease in mass velocity in the lower portion of the fuel assembly would not result in the fuel rods reaching the DNBR limit.

The open literature supports the conclusion that flow blockage in open-lattice cores, similar to the Westinghouse cores, causes flow perturbations which are local to the blockage. For example, A. Ohstubo and S. Uruwashi (Reference 76) show that the mean bundle velocity is approached asymptomatically about four inches downstream from the flow blockage in a single flow cell. Similar results were also found for two and three cells completely blocked. P. Basmer, et al., (Reference 77) tested an open-lattice fuel assembly in which 41 percent of the subchannels were completely blocked in the center of the test bundle between spacer grids. Their results show that the stagnant zone behind the flow blockage essentially disappears after 1.65 L/De or about five inches for their test bundle. They also found that leakage flow through the blockage tended to shorten the stagnant zone or, in essence, the complete recovery length. Thus, local flow blockages within a fuel assembly have little effect on subchannel enthalpy rise. In reality, a local flow blockage would be expected to promote turbulence and, therefore would not likely affect DNBR at all.

Coolant flow blockages induce local cross-flows as well as promote turbulence. Fuel rod behavior is changed under the influence of a sufficiently high cross-flow component. Fuel rod vibration could occur, caused by this cross-flow component, through vortex shedding or turbulent mechanisms. If the cross-flow velocity exceeds the limit established for fluid elastic stability, large amplitude whirling results. The limits for a controlled vibration mechanism are established from studies of vortex shedding and turbulent pressure fluctuations. The cross-flow velocity required to exceed fluid elastic stability limits is dependent on the axial location of the blockage and the characterization of the cross-flow (jet flow or not). These limits are greater than those for vibratory fuel rod wear. Cross-flow velocity above the established limits can lead to mechanical wear of the fuel rods at the grid support locations. Fuel rod wear due to flow-induced vibration is considered in the fuel rod fretting evaluation as discussed in Section 4.2.

4.4.5   Testing and Verification

4.4.5.1   Tests Prior to Initial Criticality

A reactor coolant flow test is performed, as discussed in Chapter 14, following fuel loading but prior to initial criticality. Coolant loop pressure data is obtained in this test. This data allows determination of the coolant flow rates at reactor operating conditions. This test verifies that proper coolant flow rates have been used in the core thermal and hydraulic analysis.

4.4.5.2   Initial Power and Plant Operation

Core power distribution measurements are made at several core power levels, as discussed in Chapter 14. These tests are used to confirm that conservative peaking factors are used in the core thermal and hydraulic analysis.

Additional demonstration of the overall conservatism of the THINC analysis was obtained by comparing THINC predictions to in-core thermocouple measurements, as detailed WCAP-8453-A

(Reference 78). VIPRE-01 has been confirmed to be as conservative as the THINC code in Reference 83.

4.4.5.3 Component and Fuel Inspections

Inspections performed on the manufactured fuel are described in subsection 4.2.4. Fabrication measurements critical to thermal and hydraulic analysis are obtained to verify that the engineering hot channel factors in the design analyses (subsection 4.4.2.2.4) are met.

4.4.6 Instrumentation Requirements

4.4.6.1 Incore Instrumentation

The primary function of the incore instrumentation system is to provide a three-dimensional flux map of the reactor core. This map is used to calibrate neutron detectors used by the protection and safety monitoring system as well as to optimize core performance. A secondary function of the incore instrumentation system is to provide the protection and safety monitoring system with the signals necessary for monitoring core exit temperatures. This secondary function is the result of the mechanical design that groups the detectors used for generating the flux map in the same thimble as the core exit thermocouples.

The incore instrumentation system consists of incore instrument thimble assemblies, which house fixed incore detectors, core exit thermocouple assemblies contained within an inner and outer sheath assembly, and associated signal processing and data processing equipment. There are 42 incore instrument thimble assemblies: each is composed of multiple fixed incore detectors and one thermocouple.

The thimbles are inserted into the active core through the upper head and internals of the reactor vessel. The signals output from the fixed incore detectors are digitized inside containment and multiplexed out of the containment. The signal processing software integral to the incore instrumentation system allows the fixed incore detector signals to be used to calculate an accurate three-dimensional core power distribution suitable for developing calibration information for the excore nuclear instrumentation input to the overtemperature and overpower ΔT reactor trip setpoints. The system is also capable of accurately determining whether the reactor power distribution is currently within the operating limits defined in the technical specifications while the reactor is operating above approximately 20 percent of rated thermal power.

The incore instrument system data processor receives the transmitted digitized fixed incore detector signals from the signal processor and combines the measured data with analytically-derived constants, and certain other plant instrumentation sensor signals, to generate a full three-dimensional indication of nuclear power distribution in the reactor core. It also edits the three-dimensional indication of power distribution to extract pertinent power distribution parameters outputs for use by the plant operators and engineers. The data processor also generates hardcopy representations of the detailed three-dimensional nuclear power indications.

The hardware and software which performs the three-dimensional power distribution calculation are capable of executing the calculation algorithms and constructing graphical and tabular displays of core conditions at intervals of less than one minute. The software provides information to

enable the reactor operator to ascertain how the measured peaking factor performance agrees with the peaking factor performance predicted by the design model used to determine the acceptability of the fuel loading pattern. The analysis software provides information required to activate a visual alarm display to alert the reactor operator about the current existence of, or the potential for, reactor operating limit violations. The calculation algorithms are capable of determining the core average axial offset using a minimum set of the total 42 incore monitor assemblies. A minimum set of incore monitor assemblies is at least 30 operating assemblies, with at least two operating assemblies in each quadrant, prior to nuclear model calibration; and at least 21 operating assemblies, with at least two operating assemblies in each quadrant, after nuclear model calibration. The nuclear model calibration is performed after each new core load. The hardware which performs the online power distribution monitoring is configured such that a single hardware failure will not necessitate a reactor maximum power reduction or restrict normal reactor operations.

During plant operation, the incore instrument thimble assembly is positioned within the fuel assembly and exits through the top of the reactor vessel to containment. The fixed incore detector and core exit thermocouple cables are then routed to different data conditioning and processing stations. The data is processed and the results are available for display in the main control room.

4.4.6.2   Overtemperature and Overpower ΔT Instrumentation

The overtemperature ΔT trip protects the core against low DNBR. The overpower ΔT trip protects against excessive power (fuel rod rating protection).

As described in subsection 7.2.1.1.3, factors included in establishing the overtemperature ΔT and overpower ΔT trip setpoints include the reactor coolant temperature in each loop and the axial distribution of core power as seen by excore neutron detectors.

4.4.6.3   Instrumentation to Limit Maximum Power Output

The signals from the three ranges (source, intermediate, and power) of neutron flux detectors, are used to limit the maximum power output of the reactor within their respective ranges.

There are eight radial locations containing a total of twelve neutron flux detectors installed around the reactor between the vessel and the primary shield. Four proportional counters for the source range are located at the highest fluence portions of the core containing the primary startup sources at an elevation approximately one-fourth of the core height. Four pulse fission chambers for the intermediate range, located in the same instrument wells as the source range detectors, are positioned at an elevation corresponding to one-half of the core height. Four uncompensated ionization chamber assemblies for the power range are installed vertically at the four corners of the core. These assemblies are located equidistant from the reactor vessel along the length and, to minimize neutron flux pattern distortions, within approximately one foot of the reactor vessel. Each power range detector provides two signals corresponding to the neutron flux in the upper and in the lower sections of a core quadrant. The three ranges of detectors are used as inputs to monitor neutron flux from a completely shutdown condition to 120 percent of full power, with the capability of recording overpower excursions up to 200 percent of full power.

The output of the power range channels is used for:

- Protecting the core against the consequences of rod ejection accidents

- Protecting the core against the consequences of adverse power distributions resulting from dropped rods

- The rod speed control function

- Alerting the operator to an excessive power imbalance between the quadrants

The intermediate range detectors also provide signals for the post-accident monitoring system.

Details of the neutron detectors and nuclear instrumentation design and the control and trip logic are given in Chapter 7. The limits on neutron flux operation and trip setpoints are given in the technical specifications.

4.4.6.4   Digital Metal Impact Monitoring System

The digital metal impact monitoring system is a nonsafety-related system that monitors the reactor coolant system for metallic loose parts. It consists of several active instrumentation channels, each comprising a piezoelectric accelerometer (sensor), signal conditioning, and diagnostic equipment. The digital impact monitoring system conforms with Regulatory Guide 1.133.

The digital metal impact monitoring system is designed to detect a loose parts that weigh from 0.25 to 30 pounds, and can also detect impact with a kinetic energy of 0.5 foot-pounds on the inside surface of the reactor coolant system pressure boundary within three feet of a sensor.

The digital impact monitoring system consists of several redundant instrumentation channels, each comprised of a piezoelectric accelerometer (sensor), preamplifier, and signal conditioning equipment. The output signal from each accelerometer is amplified by the preamplifier and signal conditioning equipment before it is processed by a discriminator to eliminate noise and signals which are not indicative of loose part impacts. The system starts up and operates automatically.

The system facilitates performance tests, hardware integrity tests, and the recognition, location, replacement, repair and adjustment of malfunctioning components. System performance tests are made using a hammer as a tool to simulate an impact. Additional system performance testing is performed using special test modules. These modules simulate impacts and test performance of the signal processing equipment. Hardware integrity tests are also performed to verify equipment operation.

The impact detect algorithm, used by the signal processing equipment, is designed to minimize the number of false alarms. False impact detection, attributable to normal hydraulic, mechanical and electrical noise, is minimized by a number of techniques including:

- Utilizing a floating level within the impact detection algorithm. The floating level is based on signal levels not characteristic of an impact, and is generally a function of the background noise level.

- Comparing the impact event with the times and type of normally occurring plant operation events received from plant control system such as a control rod stepping.

- Comparing the number of events detected within a given time interval.

The sensors of the impact monitoring system are fastened mechanically to the reactor coolant system at potential loose part collection regions including the upper and lower head region of the reactor pressure vessel, and the reactor coolant inlet region of each steam generator.

The equipment inside the containment is designed to remain functional through an earthquake of a magnitude equal to 50 percent of the calculated safe shutdown earthquake and normal environments (radiation, vibration, temperature, humidity) anticipated during the operating lifetime. The instrument channels associated with the sensors at each reactor coolant system location are physically separated from each other starting at the sensor locations to a point in the plant that is always accessible for maintenance during full-power operation.

The digital metal impact monitoring system is calibrated prior to plant startup. Capabilities exist for subsequent periodic online channel checks and channel functional tests and for offline channel calibrations at refueling outages.

4.4.7   Combined License Information

Combined License applicants referencing the AP1000 certified design will address changes to the reference design of the fuel, burnable absorber rods, rod cluster control assemblies, or initial core design from that presented in the DCD.

Following selection of the actual plant operating instrumentation and calculation of the instrumentation uncertainties of the operating plant parameters as discussed in subsection 7.1.6, Combined License applicants will calculate the design limit DNBR values using the RTDP with these instrumentation uncertainties and confirm that either the design limit DNBR values as described in Section 4.4, "Thermal and Hydraulic Design," remain valid, or that the safety analysis minimum DNBR bounds the new design limit DNBR values plus DNBR penalties, such as rod bow penalty.

4.4.8   References

1. ANSI N18.2a-75, "Nuclear Safety Criteria for the Design of Stationary Pressurized Water Reactor Plants."

2. Friedland, A. J. and Ray, S., "Revised Thermal Design Procedure," WCAP-11397-P-A (Proprietary) and WCAP-11397-A (Non-Proprietary), April 1989.

3. Christensen, J. A., Allio, R. J., and Biancheria, A., "Melting Point of Irradiated UO_2," WCAP-6065, February 1965.

4. Davidson, S. L. and Kramer, W. R. (Ed.), "Reference Core Report VANTAGE 5 Fuel Assembly," WCAP-10444-P-A (Proprietary) and WCAP-10445-NP-A (Non-Proprietary), September 1985.

5. Tong, L. S., "Boiling Crisis and Critical Heat Flux," AEC Critical Review Series, TID-25887, 1972.

6. Tong, L. S., "Critical Heat Fluxes in Rod Bundles, Two Phase Flow and Heat Transfer in Rod Bundles," Annual Winter Meeting ASME, November 1968, p. 3146.

7. Letter from A. C. Thadani (NRC) to W. J. Johnson (Westinghouse), January 31, 1989, Subject: Acceptance for Referencing of Licensing Topical Report, WCAP-9226-P/9227-NP, "Reactor Core Response to Excessive Secondary Steam Releases."

8. Motley, F. E., Cadek, F. F., "DNB Test Results for R-Grid Thimble Cold Wall Cells," WCAP-7695-L Addendum 1, October 1972.

9. Davidson, S. L. (Ed.), "Westinghouse Fuel Criteria Evaluation Process," WCAP-12488-A, October 1994.

10. Tong, L. S., "Prediction of Departure from Nucleate Boiling for an Axially Nonuniform Heat Flux Distribution," Journal of Nuclear Energy 21, pp 241-248, 1967.

11. Reference deleted

12. Cadek, F. F., Motley, F. E., and Dominicis, D. P., "Effect of Axial Spacing on Interchannel Thermal Mixing with the R Mixing Vane Grid," WCAP-7941-P-A (Proprietary) and WCAP-7959-A (Non-Proprietary), January 1975.

13. Rowe, D. S., and Angle, C. W., "Crossflow Mixing Between Parallel Flow Channels During Boiling, Part II Measurements of Flow and Enthalpy in Two Parallel Channels," BNWL-371, Part 2, December 1967.

14. Rowe, D. S., and Angle, C. W., "Crossflow Mixing Between Parallel Flow Channels During Boiling, Part III Effect of Spacers on Mixing Between Two Channels," BNWL-371, Part 3, January 1969.

15. Gonzalez-Santalo, J. M., and Griffith, P., "Two-Phase Flow Mixing in Rod Bundle Subchannels," ASME Paper 72-WA/NE-19.

16. Motley, F. E., Wenzel, A. H., and Cadek, F. F., "The Effect of 17 x 17 Fuel Assembly Geometry on Interchannel Thermal Mixing," WCAP-8298-P-A (Proprietary) and WCAP-8290A (Non-Proprietary), January 1975.

17. Hill, K. W., Motley, F. E., and Cadek, F. F., "Effect of Local Heat Flux Spikes on DNB in Non Uniform Heated Rod Bundles," WCAP-8174 (Proprietary), August 1973, and WCAP-8202 (Non-Proprietary), August 1973.

18. Cadek, F. F., "Interchannel Thermal Mixing with Mixing Vane Grids," WCAP-7667-P-A (Proprietary) and WCAP-7755-A (Non-Proprietary), January 1975.

19. Skaritka, J., Ed, "Fuel Rod Bow Evaluation," WCAP-8691, Revision 1 (Proprietary) and WCAP-8692, Revision 1 (Non-Proprietary), July 1979.

20. "Partial Response to Request Number 1 for Additional Information on WCAP-8691, Revision 1," Letter from E. P. Rahe, Jr. (Westinghouse) to J. R. Miller (NRC), NS-EPR-2515, October 9, 1981; "Remaining Response to Request Number 1 for Additional Information on WCAP-8691, Revision 1," Letter from E. P. Rahe, Jr. (Westinghouse) to R. J. Miller (NRC), NS-EPR-2572, March 16, 1982.

21. Letter from C. Berlinger (NRC) to E. P. Rahe, Jr. (Westinghouse), Subject: "Request for Reduction in Fuel Assembly Burnup Limit for Calculations of Maximum Rod Bow Penalty," June 18, 1986.

22. Hochreiter, L. E., "Applications of the THINC-IV Program to PWR Design," WCAP-8054-P-A (Proprietary), February 1989 and WCAP-8195 (Non-Proprietary), October 1973.

23. Hochreiter, L. E., Chelemer, H., and Chu, P. T., "THINC-IV, An Improved Program for Thermal-Hydraulic Analysis of Rod Bundle Cores," WCAP-7956-P-A, February 1989.

24. Dittus, F. W., and Boelter, L. M. K., "Heat Transfer in Automobile Radiators of the Tubular Type," California University Publication in Engineering 2, No. 13, 443461, 1930.

25. Weisman, J., "Heat Transfer to Water Flowing Parallel to Tube Bundles," Nuclear Science Engineering 6, pp 78-79, 1959.

26. Thom, J. R. S., et al., "Boiling in Subcooled Water During Flowup Heated Tubes or Annuli," Proceedings of the Institution of Mechanical Engineers 180, Part C, pp 226-246, 1955-1966.

27. Reference deleted

28. Reference deleted

29. Reference deleted

30. Kjaerheim, G., and Rolstad, E., "In-Pile Determination of UO_2, Thermal Conductivity, Density Effects, and Gap Conductance," HPR-80, December 1967.

31. Kjaerheim, G., In-Pile Measurements of Center Fuel Temperatures and Thermal Conductivity Determination of Oxide Fuels, Paper IFA-175 Presented at the European Atomic Energy Society Symposium on Performance Experience of Water-Cooled Power Reactor Fuel, Stockholm, Sweden, October 1969.

32. Cohen, I., Lustman, B., and Eichenberg, D., "Measurement of the Thermal Conductivity of Metal-Glad Uranium Oxide Rods During Irradiation," WAPD-228, 1960.

33. Clough, D. J., and Sayers, J. B., "The Measurement of the Thermal Conductivity of UO_2, under Irradiation in the Temperature Range 150 to 1600°C," AERE-4690, UKAEA Research Group, Harwell, December 1964.

34. Stora, J. P., et al., "Thermal Conductivity of Sintered Uranium Oxide under In-Pile Conditions," EURAEC-1095, 1964.

35. Devold, I., "A Study of the Temperature Distribution in UO_2, Reactor Fuel Elements," AE-318, Aktiebolaget Atomenergi, Stockholm, Sweden, 1968.

36. Balfour, M. G., Christensen, J. A., and Ferrari, H. M., "In-Pile Measurement of UO_2 Thermal Conductivity," WCAP-2923, 1966.

37. Howard, V. C., and Gulvin, T. G., "Thermal Conductivity Determinations on Uranium Dioxide by a Radial Flow Method," UKAEA IG-Report 51, November 1960.

38. Lucks, C. F., and Deem, H. W., "Thermal Conductivity and Electrical Conductivity of UO_2," in Progress Reports Relating to Civilian Applications, BMI-1448 (Revised) for June 1960, BMI-1489 (Revised) for December 1960, and BMI-1518 (Revised) for May 1961.

39. Daniel, J. L., Matolich, J. Jr., and Deem, H. W., "Thermal Conductivity of UO_2," HW-69945, September 1962.

40. Feith, A. D., "Thermal Conductivity of UO_2 by a Radial Heat Flow Method," TID-21668, 1962.

41. Vogt, J., Grandel, L., and Runfors, U., "Determination of the Thermal Conductivity of Unirradiated Uranium Dioxide," AB Atomenergi Report RMB-527, 1964, Quoted by IAEA Technical Report Series No. 59, "Thermal Conductivity of Uranium Dioxide."

42. Nishijima, T., Kawada, T., and Ishihata, A., "Thermal Conductivity of Sintered UO_2 and $4Al_2O_3$ at High Temperatures," Journal of the American Ceramic Society 48, pp 31-44, 1965.

43. Ainscough, J. B., and Wheeler, M. J., "Thermal Diffusivity and Thermal Conductivity of Sintered Uranium Dioxide," Proceedings of the Seventh Conference of Thermal Conductivity, National Bureau of Standards, Washington, p 467, 1968.

44. Godfrey, T. G., et al., "Thermal Conductivity of Uranium Dioxide and Armco Iron by an Improved Radial Heat Flow Technique," ORNL-3556, June 1964.

45. Stora, J. P., et al., "Thermal Conductivity of Sintered Uranium Oxide Under In-Pile Conditions," EURAEC-1095, August 1964.

46. Bush, A. J., "Apparatus for Measuring Thermal Conductivity to 2500°C," Reporting 64-1P6-401-43 (Proprietary), Westinghouse Research Laboratories, February 1965.

47. Asamoto, R. R., Anselin, F. L., and Conti, A. E., "The Effect of Density on the Thermal Conductivity of Uranium Dioxide," GEAP-5493, April 1968.

48. Kruger, O. L., <u>Heat Transfer Properties of Uranium and Plutonium Dioxide</u>, Paper 11-N-68F, presented at the Fall Meeting of Nuclear Division of the American Ceramic Society, Pittsburgh, September 1968.

49. Weiner, R. A., et al., "Improved Fuel Performance Models for Westinghouse Fuel Rod Design and Safety Evaluations," WCAP-10851-P-A (Proprietary) and WCAP-11873-A (Non-Proprietary), August 1988.

50. Leech, W. J. et al., "Revised PAD Code Thermal Safety Model," WCAP-8720, Addendum 2, October 1982.

51. Duncan, R. N., "Rabbit Capsule Irradiation of UO_2," CVTR Project, CVNA Project, CVNA-142, June 1962.

52. Nelson, R. G., et al., "Fission Gas Release from UO_2 Fuel Rods with Gross Central Melting," GEAP-4572, July 1964.

53. Gyllander, J. A., "In-Pile Determination of the Thermal Conductivity of UO_2 in the Range 500 to 2500°C," AE-411, January 1971.

54. Lyons, M. F., et al., "UO_2 Powder and Pellet Thermal Conductivity During Irradiation," GEAP-5100-1, March 1966.

55. Coplin, D. H., et al., "The Thermal Conductivity of UO_2 by Direct In-Reactor Measurements," GEAP-5100-6, March 1968.

56. Bain, A. S., "The Heat Rating Required to Produce Center Melting in Various UO_2 Fuels," ASTM Special Technical Publication No. 306, Philadelphia, pp 30-46, 1962.

57. Stora, J. P., "In-Reactor Measurements of the Integrated Thermal Conductivity of UO_2 - Effect of Porosity," <u>Transactions of the American Nuclear Society 13</u>, pp 137-138, 1970.

58. International Atomic Energy Agency, "Thermal Conductivity of Uranium Dioxide," Report of the Panel Held in Vienna, April 1965, <u>IAEA Technical Reports Series</u>, No. 59, Vienna, 1966.

59. Poncelet, C. G., "Burnup Physics of Heterogeneous Reactor Lattices," WCAP-6069, June 1965.

60. Nodvick, R. J., "Saxton Core II Fuel Performance Evaluation," WCAP-3385-56, Part II, "Evaluation of Mass Spectrometric and Radiochemical Analyses of Irradiated Saxton Plutonium Fuel," July 1970.

61. Reference deleted

62. Reference deleted

63. Reference deleted

64. Idel'chik, I. E., "Handbook of Hydraulic Resistance," 2nd Edition, Hemisphere Publishing Corp., 1986.

65. McFarlane, A. F., "Power Peaking Factors," WCAP-7912-P-A (Proprietary) and WCAP-7912-A (Non-Proprietary), January 1975.

66. Reference deleted

67. Reference deleted

68. Boure, J. A., Bergles, A. E., and Tong, L. S., "Review of Two-Phase Flow Instability," Nuclear Engineering Design 25, pp 165-192, 1973.

69. Lahey, R. T., and Moody, F. J., The Thermal Hydraulics of a Boiling Water Reactor, American Nuclear Society, 1977.

70. Saha, P., Ishii, M., and Zuber, N., "An Experimental Investigation of the Thermally Induced Flow Oscillations in Two-Phase Systems," Journal of Heat Transfer, pp 616-622, November 1976.

71. Virgil C. Summer Nuclear Station FSAR, Chapter 4, South Carolina Electric & Gas Company, Docket No. 50-395.

72. Byron/Braidwood Stations FSAR, Chapter 4, Commonwealth Edison Company, Docket No. 50-456.

73. South Texas Project Electric Generating Station FSAR, Chapter 4, Houston Lighting and Power Company, Docket No. 50-498.

74. Kakac, S., et al., "Sustained and Transient Boiling Flow Instabilities in a Cross-Connected Four-Parallel-Channel Upflow System," Proceedings of Fifth International Heat Transfer Conference, Tokyo, September 1974.

75. Kao, H. S., Morgan, T. D., and Parker, W. B., "Prediction of Flow Oscillation in Reactor Core Channel," Transactions of the American Nuclear Society 16, pp 212-213, 1973.

76. Ohtsubo, A., and Uruwashi, S., "Stagnant Fluid Due to Local Flow Blockage," Journal of Nuclear Science Technology, No. 7, pp 433-434, 1972.

77. Basmer, P., Kirsh, D., and Schultheiss, G. F., "Investigation of the Flow Pattern in the Recirculation Zone Downstream of Local Coolant Blockages in Pin Bundles," Atomwirtschaft 17, No. 8, pp 416-417, 1972 (in German).

78. Burke, T. M., Meyer, G. E., and Shefcheck, J., "Analysis of Data from the Zion (Unit 1) THINC Verification Test," WCAP-8453-A, May 1976.

79. Reference deleted

80.   Reference deleted

81.   Davidson, S. L., and Ryan, T. L., "VANTAGE+ Fuel Assembly Reference Core Report," WCAP-12610-P-A (Proprietary) and WCAP-14342-A (Non-Proprietary), April 1995.

82.   Smith, L. D., et al., "Modified WRB-2 Correlation, WRB-2M, for Predicting Critical Heat Flux in 17x17 Rod Bundles with Modified LPD Mixing Vane Grids," WCAP-15025-P-A (Proprietary) and WCAP-15026-NP (Non-Proprietary), April 1999.

83.   Sung, Y. X., et al., "VIPRE-01 Modeling and Qualification for Pressurized Water Reactor Non-LOCA Thermal-Hydraulic Safety Analysis," WCAP-14565-P-A and WCAP-15306-NP-A, October 1999.

84.   Stewart, C. W., et al., "VIPRE-01: A Thermal-Hydraulic Code for Reactor Core," Volume 1-3 (Revision 3, August 1989), Volume 4 (April 1987), NP-2511-CCM-A, Electric Power Research Institute.

85.   Slagle, W. H. (ed.) et al., "Westinghouse Improved Performance Analysis and Design Model (PAD 4.0)," WCAP-15063-P-A, Revision 1 (Proprietary) and WCAP-15064-NP-A, Revision 1 (Non-Proprietary), July 2000.

86.   Kitchen, T. J., "Generic Safety Evaluation for 17x17 Standard Robust Fuel Assembly (17x17 STD RFA)," SECL-98-056, Revision 0, September 30, 1998.

87.   WCAP-16652-NP, "AP1000 Core & Fuel Design Technical Report," Revision 0.

Table 4.4-1 (Sheet 1 of 2)		
THERMAL AND HYDRAULIC COMPARISON TABLE **(AP1000, AP600 AND A TYPICAL WESTINGHOUSE XL PLANT)**		
Design Parameters	**AP1000[a]**	**AP600**	**Typical XL Plant**
Reactor core heat output (MWt)	3400	1933	3800
Reactor core heat output (10^6 BTU/hr)	11601	6596	12,969
Heat generated in fuel (%)	97.4	97.4	97.4
System pressure, nominal (psia)	2250	2250	2250
System pressure, minimal (psia)	2190	2200	2204

Minimum DNBR at nominal conditions
    Typical flow channel
    Thimble (cold wall) flow channel)
	
	 2.80
	 2.74
		
		 3.48
		 3.33
			
			 2.20
			 2.12

Minimum DNBR for design transients
    Typical flow channel
    Thimble (cold wall)flow channel
	
	 >1.25[b] >1.22[b]
	 >1.25[b] >1.21[b]
		
		 >1.23
		 >1.22
			
			 >1.26
			 >1.24

DNB correlation[c]	WRB-2M	WRB-2	WRB-1

Coolant conditions[d]
   Vessel minimum measured flow rate (MMF)
     10^6 lbm/hr
     gpm
   Vessel thermal design flow rate (TDF)
     10^6 lbm/hr
     gpm
   Effective flow rate for heat transfer[e]
     10^6 lbm/hr
     gpm
   Effective flow area for heat transfer (ft^2)
     Average velocity along fuel rods (ft/s)[e]
     Average mass velocity, 10^6 lbm/hr-ft^{2}[e]
	
	 115.55
	 301,670
	
	 113.5
	 296,000
	
	 106.8
	 278,500
	 41.8
	 15.8
	 2.40
		
		 74.4
		 193,200
		
		 72.9
		 189,600
		
		 66.3
		 172,500
		 38.5
		 10.6
		 1.72
			
			 148.9
			 403,000
			
			 145.0
			 392,000
			
			 132.7
			 358,700
			 51.1
			 16.6
			 2.60

Coolant Temperature[d][e]
   Nominal inlet (°F)
   Average rise in vessel (°F)
   Average rise in core (°F)
   Average in core (°F)
   Average in vessel (°F)
	
	 535.0
	 77.2
	 81.4
	 578.1
	 573.6
		
		 532.8
		 69.6
		 75.8
		 572.6
		 567.6
			
			 561.2
			 63.6
			 68.7
			 597.8
			 593.0

Table 4.4-1 (Sheet 2 of 2)

**THERMAL AND HYDRAULIC COMPARISON TABLE
(AP1000, AP600 AND A TYPICAL WESTINGHOUSE XL PLANT)**

Design Parameters	AP1000[a]	AP600	Typical XL Plant
Heat transfer			
Active heat transfer surface area $(ft^2)^{(f)}$	56,700	44,884	69,700
Average heat flux $(BTU/hr\text{-}ft^2)$	199,300	143,000	181,200
Maximum heat flux for normal operation $(BTU/hr\text{-}ft^2)^{(g)}$	518,200	372,226	498,200
Average linear power $(kW/ft)^{(f)}$	5.72	4.11	5.20
Peak linear power for normal operation $(kW/ft)^{(g,h)}$	14.9	10.7	14.0
Peak linear power resulting from overpower transients/operator errors, assuming a maximum overpower of 118% $(kW/ft)^{(h)}$	$\leq$22.45	22.5	$\leq$22.45
Peak Linear power for prevention of center-line melt $(kW/ft)^{(i)}$	22.5	22.5	22.45
Power density (kW/l of core)$^{(j)}$	109.7	78.82	98.8
Specific power (kW/kg uranium)$^{(j)}$	40.2	28.89	36.6
Fuel central temperature			
Peak at peak linear power for prevention of centerline melt (°F)	4700	4,700	4700
Pressure drop$^{(k)}$			
Across core (psi)	39.9 $\pm$ 4.0$^{(l)}$	17.5 $\pm$ 1.7	38.8 $\pm$ 3.9
Across vessel, including nozzle (psi)	62.3 $\pm$ 6.2$^{(l)}$	45.3 $\pm$ 4.5	59.7 $\pm$ 6.0

Notes:

(a) Robust Fuel Assembly.

(b)   1.25 applies to Core and Axial Offset limits; 1.22 and 1.21 apply to all other RTDP transients.

(c) WRB-2M is used for AP1000. WRB-2 or W-3 is used for AP1000 where WRB-2M is not applicable. See subsection 4.4.2.2.1 for use of W-3, WRB-2 and WRB-2M correlations.

(d) Based on vessel average temperature equal to 573.6°F. Flow rates and temperatures based on 10 percent steam generator tube plugging.

(e) Based on thermal design flow and 5.9 percent bypass flow.

(f) Based on densified active fuel length. The value for AP1000 is rounded to 5.72 kW/ft.

(g) Based on 2.60 F_Q peaking factor.

(h) See subsection 4.3.2.2.6.

(i) See subsection 4.4.2.11.6.

(j) Based on cold dimensions and 95.5 percent of theoretical density fuel for AP1000; 95 percent for others.

(k) These are typical values based on best-estimate reactor flow rate as discussed in Section 5.1.

(l) Inlet temperature = 536.8°F.

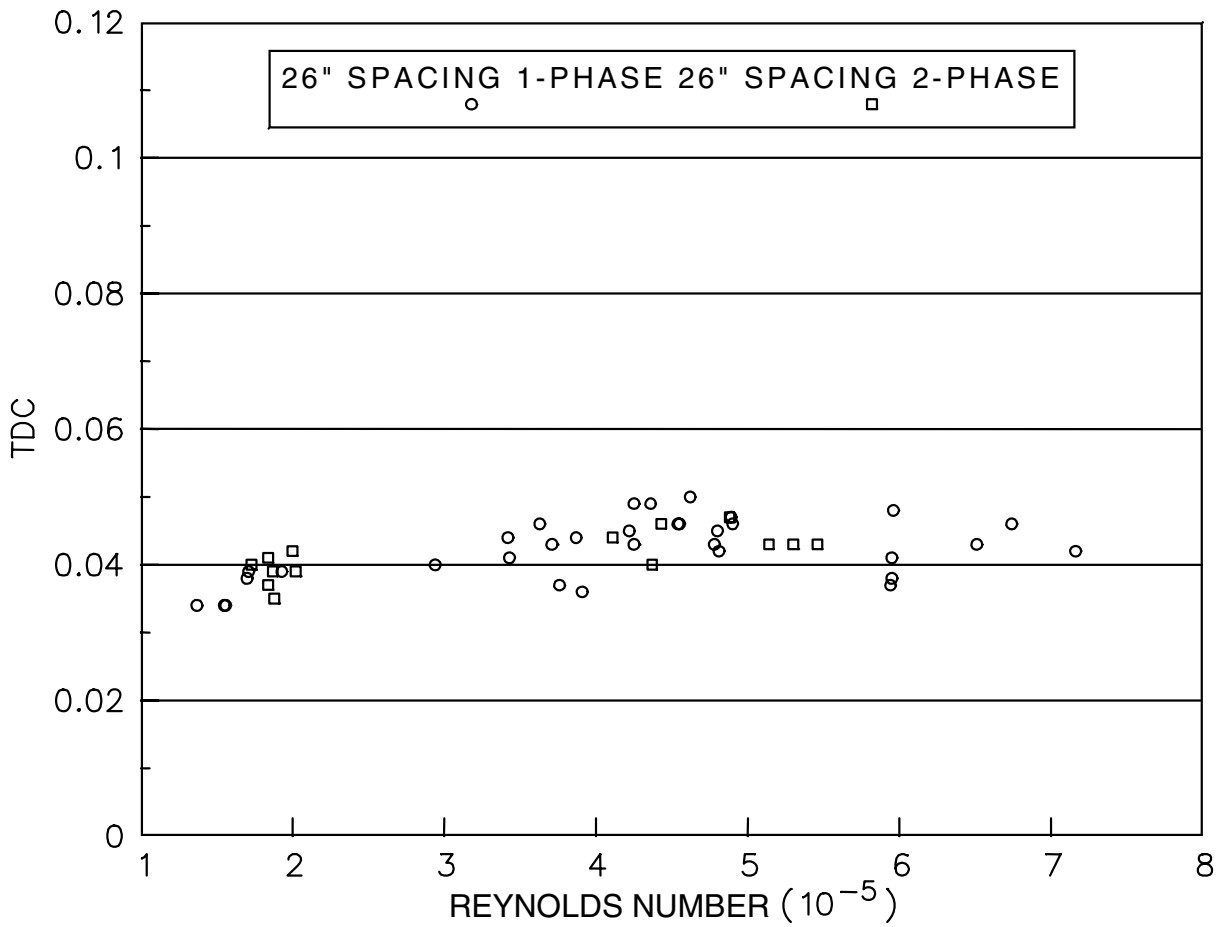| Table 4.4-2 **VOID FRACTIONS AT NOMINAL REACTOR CONDITIONS WITH DESIGN HOT CHANNEL FACTORS** **(BASED ON VIPRE-01)**		
	Average	**Maximum**
Core, %	0.0	-
Hot Subchannel, %	0.1	0.9

Figure 4.4-1

Thermal Diffusion Coefficient (TDC)
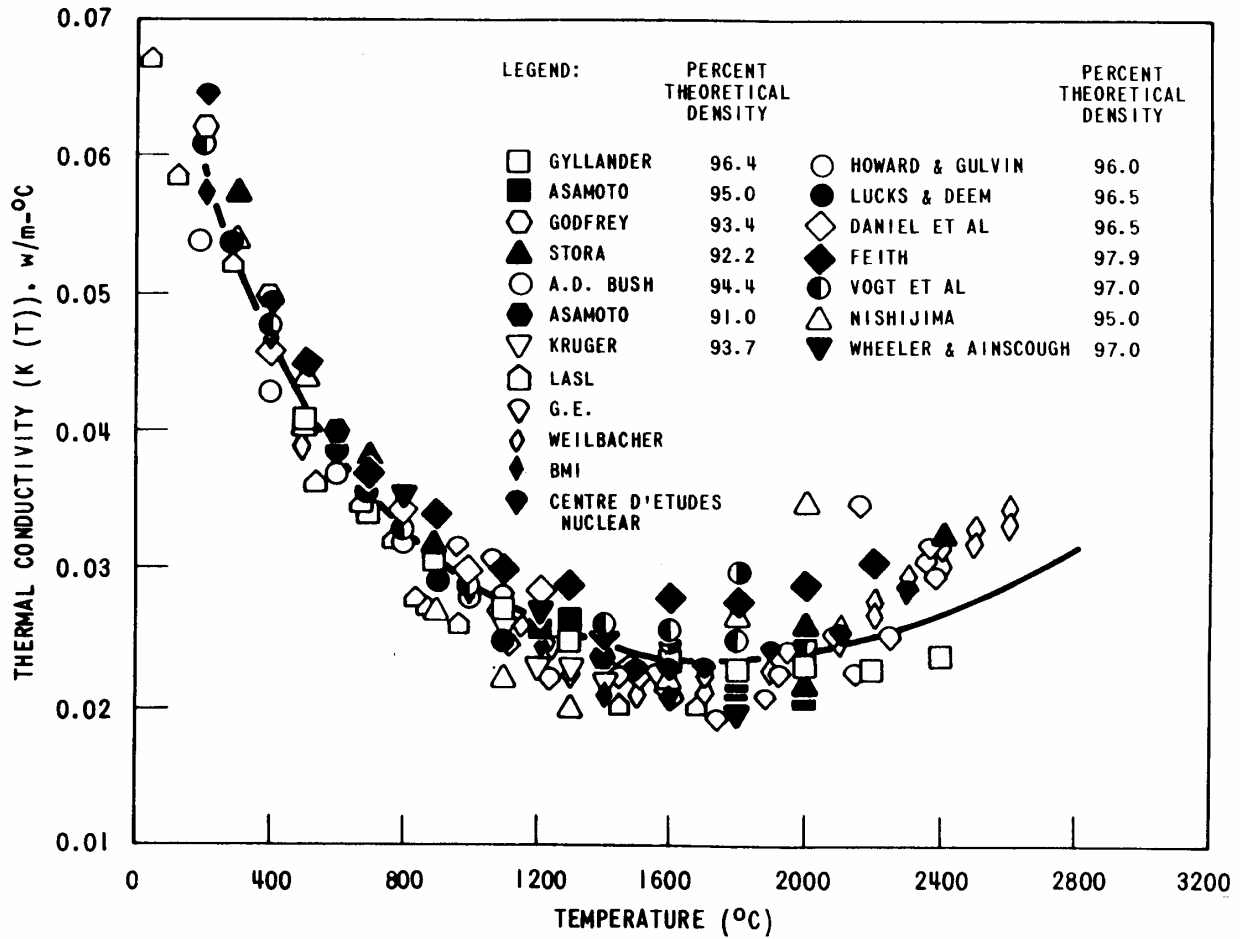**As a Function of Reynolds Number**

Figure 4.4-2

Thermal Conductivity of Uranium Dioxide
(Data Corrected to 95% Theoretical Density)